Heliyon 6 (2020) e05029

Contents lists available at ScienceDirect

Heliyon

journal homepage: www.cell.com/heliyon

Research article

Green synthesis of triclinic (anorthic) phase $AgCoPO_4$ nanoparticles: optical studies and theoretical modelling

Anuoluwa Abimbola Akinsiku [a,*], Olayinka Oyewale Ajani [a], Joseph Adeyemi Adekoya [a], Moses Eterigho Emetere [b], Enock Olugbenga Dare [c,**]

[a] Department of Chemistry, Covenant University, Nigeria
[b] Department of Physics, Covenant University, Nigeria
[c] Federal University of Agriculture Abeokuta, Nigeria

ARTICLE INFO

Keywords:
Materials chemistry
Nanotechnology
$AgCoPO_4$ phase
Optical properties
Anisotropy
Triclinic
Green chemistry

ABSTRACT

We report the plant-mediated synthesis, structural investigation, optical properties and theoretical modelling of a triclinic (anorthic) phase $AgCoPO_4$ nanoparticles for the first time. As part of green chemistry, the secondary metabolites in the leaf extract of *Canna indica* were engaged as the reducing/capping agent for the metal nanoparticles. X-ray diffraction (XRD) revealed the presence of an anorthic $AgCoPO_4$ phase, crystallised in a triclinic structure with P -1 space group. Optical studies using UV-vis spectroscopy and photoluminescence are reported. Transmission electron microscopy suggests the formation of quasi-nanocube morphology, unlike the conventional spherically-shaped nanoparticles via plant-mediated reduction method. Elemental composition of the nanohybrid was confirmed by energy-dispersive x-ray spectroscopy (E.D.S.). Evidence of crystallinity was supported by selected area electron diffraction (SAED). Study of the dynamic anisotropy of the nanohybrid at optimised state suggests its proposed application as optical material in colourimetric metal nanoparticles-mediated sensors.

1. Introduction

Sustainable nanotechnology and application of the knowledge of green chemistry have led to cutting-edge research today. Given this, there is a need to focus research attention on procedures that are safe for both human health and the environment. Awareness and engagement of under-utilised biodiversity are now gaining attention, especially in nanoscience research and development. Also, methods of synthesising nanoparticles (N.P.s) using biological routes include the use of plant extract, microorganisms (algae, fungi and enzymes) [1,2], pigeon excreta, among others [3]. However, the green procedure of metallic nanoparticles involving the use of biodiversity plant as a reducing/-stabilising agent is of many advantages. Merits of phytosynthesis of metal nanoparticles include rapid synthesis, cost-effectiveness, sustainability, reproductivity of procedures, elimination of toxic chemicals, high temperature, pressure and energy [4,5]. Moreover, the use of plant extract as a reducing agent provide capping and stability for the newly formed metal nanoparticles instead of toxic chemicals [6]. The protocol is also not a complicated one, thereby requiring multi-steps of purification. Reduction of metal ions is possible as a result of active secondary metabolites like tannins, alkaloids, saponins, terpenoids etc. existing in the plant extracts [7,8], which contains healing therapeutic properties, unlike nanoparticles from chemical methods. Therefore, the ability to produce nanomaterial using herbal and plant extracts opened up a new vista of opportunity and new research focus. Reports have shown that even the wastes generated via plant-mediated synthesis of nanoparticles are environmentally friendly compared with the classical wet-chemical fabrication methods [9]. Also, typical methods of synthesising metallic nanoparticles are often time-consuming, unlike green protocol [10,11]. Due to the high demand of products of nanoparticles and nanomaterials; production of environmentally friendly and cost-effective nanomaterials is a necessity [12,13].

Triclinic (anorthic), one of the seven (7) crystal systems are categorised by vectors of unequal length and different angles i. e. ($a \neq b \neq c$ and $\alpha \neq \beta \neq \gamma$), e.g. orthorhombic system [14]. Researchers have identified materials with triclinic phase, e.g., Ling et al. (2017) [15] differentiated a triclinic and hexagonal birnessite using spectroscopy techniques of Fourier transform infra-red and x-ray diffraction for a

* Corresponding author.
** Corresponding author.
E-mail addresses: anu.akinsiku@covenantuniversity.edu.ng (A.A. Akinsiku), dare3160@hotmail.com (E.O. Dare).

https://doi.org/10.1016/j.heliyon.2020.e05029
Received 16 August 2019; Received in revised form 24 July 2020; Accepted 18 September 2020

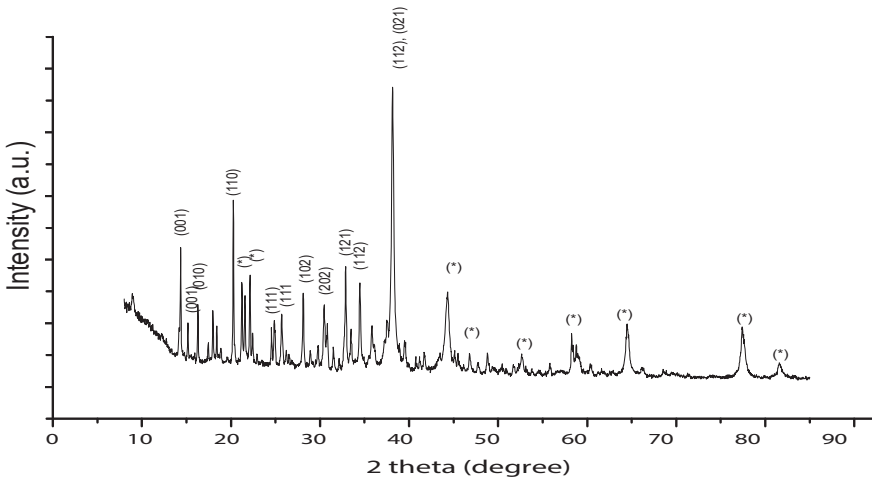

Figure 1. XRD patterns of triclinic phase $AgCoPO_4$ formed using the extract of *C. indica* leaves.

biogenic material. Fe doped WO3 film characterised to be triclinic hexagonal phase was used for photocatalytic reduction of Chromium (VI) by Feng et al. (2019) [16]. However, several works of literature show that synergistic properties of nanoparticles as a result of mixing and geometrical patterns display astonishing new features which augment their functionality and application [17,18]. They exhibit unique electronic, catalytic and optical properties compared with their corresponding monometallic nanoclusters [19, 20, 21, 22, 23]. Large surface area to volume ratio possessed by metallic nanoparticles (N.P.s) and their composite materials enable their applications in various fields. Optical materials could also be developed from metallic N.P.s due to possession of novel characteristics like photoluminescence properties, photonic crystal and plasmon resonance. Non-linear optical property present in silver (AgNPs) nanoparticles is as a result of confine excitons leading to quantum effect [24]. Essential facts about Ag NPs is their ability to tune surface plasmon resonance (S.P.R.) peak wavelengths from violet light (400 nm) to green light (530 nm) for varieties of applications in lighting, optoelectronics, photovoltaic, biomedical and thermoelectric [25]. Applications of such materials are in the chip-technology when materials are reduced to the smallest confines [26,27]. It is worth noting that metallic nanomaterials are optically active based on their photoluminescence emission, absorption and non-linear properties.

From literature, the crystal structure of $AgCoPO_4$ had been solved using Patterson and direct method [28]. So far, preparation of Ag–Co nanoparticles via physical and chemical method was reported [29, 30, 31]; however, few findings were carried out using the plant-influenced green approach. Studies showed that the existence of rare metal is known to enhance the stability of cobalt against oxidation [32]. Anuar & Andas (2016) [33] reported. Synthesis and characterisation of Co, Ag and Ag/Co nanoparticles using extracted silica from rice husk. Practical applications of the biosynthesised nanoparticles are now on the increase; for instance, Ag nanoparticles are widely and already used as an antimicrobial agent both in medicines and consumer products [34]. Besides, Bagherzade et al. (2018) [35] utilised and engaged the antibacterial activity of *Crocus sativus* wastages to synthesise AgNPs against bacteria. The catalytic action of plant-mediated silver nanoparticles was also involved in the reduction of methylene blue dye [36]. It is noteworthy that the use of hybrid N.P.s is hopeful in nanomedicine for drug delivery [11,37]. Applications of nanoparticles with core-shell structures have also been identified in biomedical engineering [38], as an electromagnetic booster in surface-enhanced spectroscopy due to S.P.R. effect [39].

As far as we know, no work has published a synthesis of triclinic (anorthic) phase $AgCoPO_4$ nanoparticles using the aqueous extract of Indian shot as a bio-reducing agent. Hence, this study focused on the fabrication of $AgCoPO_4$ nanohybrid from silver and cobalt precursors; reduced and stabilised by using eco-friendly leaf extract of *Canna indica*. The morphological and optical properties of the as-prepared nanohybrid also were explored.

2. Experimental

2.1. Materials

Silver nitrate ($AgNO_3$) and cobalt chloride hexahydrate ($CoCl_2.6H_2O$) (Sigma-Aldrich Corporation, U.K.), used as received. Leaf extract of *Canna indica* (Indian shot), filter paper (Whatman no.1) and distilled-deionised water (d-d water).

2.2. Preparation of aqueous leaf extract

Indian shot leaves were obtained in the university vicinity and prepared by modifying previous works [40,41]. Dust and impurities were removed from the leaves by thorough washing with d-d water, chopped and then homogenised using a clean blender. Extraction was carried out using a modified method from previous work [42], weight/volume fraction of 1:10, and distilled de-ionised water as solvent medium (Part of 'green' study), as used in previous work [43]. The slurry obtained was then separated with filter paper (Whatman no.1), and conserved at 4 °C for qualitative analysis and nanohybrid synthesis.

2.3. Qualitative analysis of Canna indica leaf extract

Phytochemical screening to detect chemical compounds present in *Canna indica* extract was carried out using a standard technique [44,45].

2.4. Synthesis of $AgCoPO_4$ phase nanohybrid

$AgCoPO_4$ phase nanoparticles were synthesised by a modification to previous works [46,47], using plant-extract reduction method. Filtrate (24 mL) of *Canna indica* leaf extract was mixed with equimolar concentration mixture of 120 mL $AgNO_3$ and 120 mL $CoCl_2.6H_2O$ in a beaker at varied precursor concentrations (1.0–2.0 mM). The original colour of the reaction was noted. The reaction mixture was stirred repeatedly with gradual heating to 80 °C on a hotplate until the reaction colour changed. Aliquots of the reaction mixture were taken out at different times for absorbance measurements.

2.5. Isolation of the nanohybrid

Nanoparticles were isolated using Thermo Fisher Scientific Centrifuge (Thermo Electron L.E.D.), at 7000 revolutions per minute for 40 min. Several washes were carried out on the resulted nanoparticles as the

Table 1. Comparison between match analysis and Rietveld refinement.

	a (Å)	b (Å)	c (Å)	α	β	γ
Unit cell analysis	9.5160	5.5470	6.5720	102.330°	106.270°	80.130°
Rietveld Refinement value	9.49016	5.43855	6.66219	105.063	106.725	80.1936

residual nanoparticles were redispersed in distilled-deionised water to eliminate any organics present. This procedure was repeated many times, and centrifugation was done each time the process was repeated on the dispersed solution until the $AgCoPO_4$ dispersion solution formed became clearer. The product was dried in the oven before further characterisations.

2.6. Characterisation

Optical analyses were carried out with a double beam Thermo scientific Genesys 10s UV-vis spectrophotometer and Perkin-Elmer 55 luminescence spectrophotometer. The aliquot samples taken at different times were placed in a quartz cell (1 cm path length) of a UV-vis spectrophotometer. Structural investigation of the bio-synthesised nanohybrid was carried out using x-ray diffraction (XRD) at room temperature, the scanning rate of $0.05°min^{-1}$, and 2θ range of 20^0 - 80^0 on a Bruker A.X.S. D8 diffractometer equipped with nickel filtered Cu Ka radiation (k = 1.5418 Å) at 40 kV, 40 mA. The detailed structure, morphology and particle size were verified with Technai G2 transmission electron microscope (T.E.M.) attached with an energy-dispersive x-ray spectrometer (E.D.S.), operated at an accelerating voltage of 200 KeV and 20 μA current. Evidence of crystallinity was studied with selected area electron diffraction (SAED).

3. Results and discussion

3.1. Phase analysis

Crystalline structure and phase purity of the as-prepared nanoparticles was studied via x-ray diffraction (XRD) investigation, which was collected over a range of 10–80° at an angular resolution 0.05° (Figure 1). The reflection peaks at 2θ values of 14.38° (001), 15.19° (001), 16.29° (010), 20.26° (110), 24.84° (111), 25.66° (111), 28.14° (102), 30.43° (202), 32.86° (121), 34.51° (112), 35.80° (112) and 35.19° (112, 021) confirmed the formation of triclinic (anorthic) phase $AgCoPO_4$ nanoparticles (Figure 1). The diffraction peaks show triclinic phase $AgCoPO_4$ with a space group of P-1 (ICDD# 96-100-7138). The unidentified peaks plausibly indicate phase impurity, which is further corroborated by E.D.X. analysis (Table 1), as a result of the nature of bio-reducing agent used, similar to reported study [2]. In Figure 1, the crystallite size of the as-prepared triclinic phase $AgCoPO_4$ nanoparticles was derived from the Debye-Scherrer equation:

$$D = K\lambda/d\cos\theta$$

where θ = Bragg angle
λ = X-ray wavelength

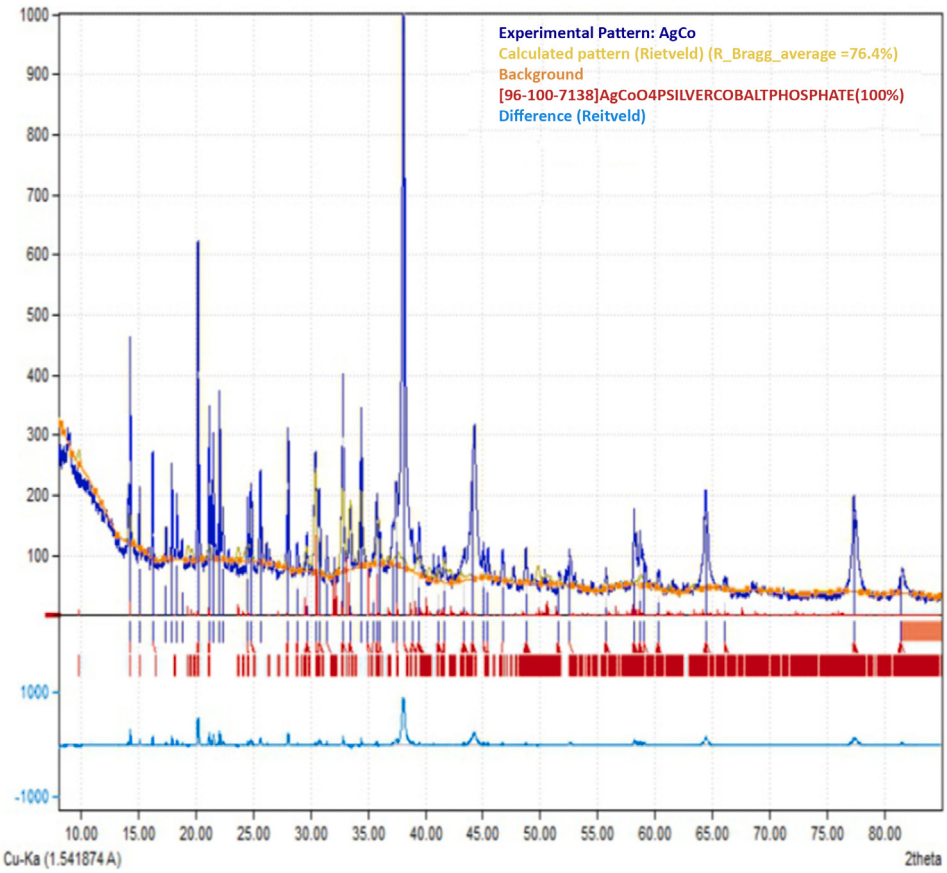

Figure 2. XRD pattern of triclinic (anorthic) phase $AgCoPO_4$ nanoparticles.

Table 2. Structural parameter derived from Rietveld's refinements of $AgCoPO_4$ XRD pattern.

	Triclinic (anorthic): $AgCoPO_4$			
Cell parameters	Space group			
	a (Å)	9.5160 Å		
	b (Å)	5.5470 Å		
	c (Å)	6.5720 Å		
	α	102.330°		
	β	106.270°		
	γ	80.130°		
Atomic positions				
		x	y	z
	Ag1_ph1	0.11878	0.33457	0.37342
	Ag2_ph1	0.24864	0.84128	0.47953
	Co3_ph1	0.42991	0.21377	0.16703
	Co4_ph1	0.21209	0.67798	0.93963
	P5_ph1	0.4643	0.3216	0.7139
	P6_ph1	0.0931	0.1809	0.8534
	O7_ph1	0.4426	0.1311	0.8388
	O8_ph1	0.6305	0.3602	0.7769
	O9_ph1	0.4076	0.2364	0.473
Final weighted average Bragg R-factor	76.4			

Table 3. The E.D.X analysis.

Element	series	[wt.%]	[norm. wt.%]	[norm. at. %]	Error in %
Silver	L-series	32.49	53.99	52.48	1.40
Oxygen	K-series	9.43	6.61	6.47	6.12
Carbon	K-series	9.21	2.80	9.52	0.40
Nickel	K-series	0.10	0.81	1.34	0.12
Cobalt	K-series	20.10	32.13	30.06	0.04
Phosphorus	K-series	0.47	1.68	0.57	0.05
Sulphur	K-series	0.11	1.60	0.13	0.04
	Sum:	71.91	100.00	100.00	

d = FWHM in radians
K = 0.94

Moreover, the observed sharp peaks (Figure 1) indicate highly-crystalline grains. Phosphate in the structure originates from terpenoid in the plant extract via terpenoid-geranyl pyrophosphate, which is a precursor to all terpene and terpenoids present [48]. The structure refinement for ICDD# 96-100-7138 was examined by the Rietveld analysis using FullProf software, which disclosed the presence of an anorthic $AgCoPO_4$ phase, crystallised in a triclinic structure with P -1 space group. From the refinement of the crystal structure by the Rietveld analysis using Fullprof software, the analysis showed an amount of 70.57% peak intensity belonging to selected phases, while the remaining 29.43% could plausibly be as a result of impurity phase as reported in previous work [2]. The obtained values of the refined occupancy states in the triclinic phase are with cell; a = 9.5160 Å, b = 5.5470 Å, c = 6.5720 Å, α = 102.330°, β = 106.270° and γ = 80.130° matched with an existing crystal phase database [49]. Figure 2 shows the Rietveld refinement for our compound, indicating a good agreement between observed and calculated profiles. Detailed result of the refinement is presented in Tables 2 and 3. The phase match exhibits specimen displacement correction (Bragg-Brentano geometry) T = (-s/R) = 0.00020784 using x-ray radiation, at 1.541874 Å wavelength. See supplementary (S1) and Mendeley data repository for the X.R.D. data [50].

3.2. Qualitative analysis

Qualitative analysis carried out on the aqueous leaf extract of *Canna indica* indicated the presence of biochemicals which indicated the presence of terpenoids, glycosides and alkaloids [41]. Even though the extraction was carried out in an aqueous medium as part of chemistry, terpenoids, glycosides and alkaloids (secondary metabolites) present were substantial to reduce the metal ions. The proposed mechanism via terpenoid-geranyl pyrophosphate (a precursor to all terpene and terpenoids) for the formation of the hybrid nanoparticles is presented in Scheme 1.

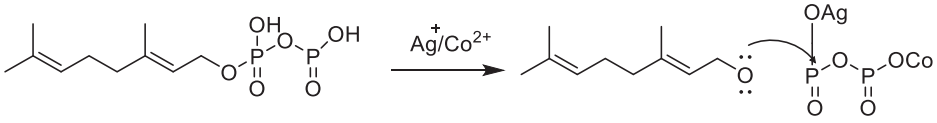

Scheme 1. Proposed mechanism of $AgCoPO_4$ NPs formation.

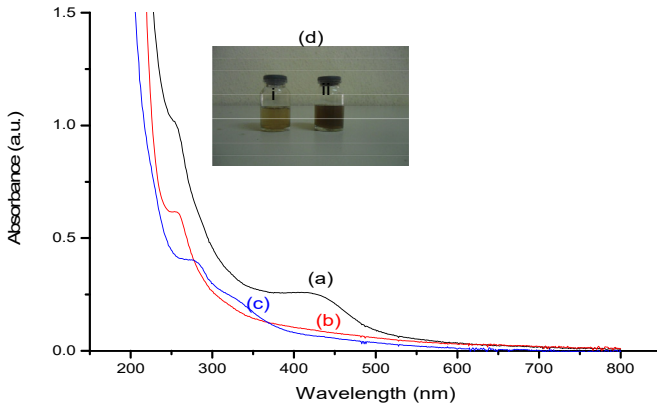

Figure 3. Absorbance spectra (a) 1.0 mM (b) 2.0 mM (c) extract (d) inset, mixture before (i) and dispersion formed after reduction (ii), of Ag–Co NPs at 80 °C, 1 h.

3.3. Optical analysis

Absorption and photoluminescence spectroscopy were used to study the optical properties of the biosynthesised nanohybrid. Extinction spectra of nanohybrid prepared using the extract of *C. indica* leaf as a bio-reducing agent are depicted by Figure 3. Visual evidence of nanoparticle formation was observed as the reaction colour changed from light brown to deep brown (Inset in Figure 3), which signalled the formation of nanoparticles similar to previous syntheses [51,52] (Figure 3a). The observed colour change could be explained as the effect of electronic transitions in metal nanoparticles due to their interaction with light. See supplementary (S2) and Mendeley data repository for the Uv-Visible absorption data.

The redox reaction involved in this process as Ag^+ was preferentially reduced because of its higher standard reduction potential compared to Co^{2+} is illustrated in the following reactions.

$$AgNO_3 \rightarrow Ag^+ + NO_3^-$$
$$CoCl_2 \rightarrow Co^{2+} + 2Cl^-$$
$$Ag^+_{(aq)} + e^- \rightarrow Ag^0_{(s)} \quad (E_{reduction} = +0.80\text{V})$$
$$Co^{2+}_{(aq)} + 2e \rightarrow Co^0_{(s)} \quad (E_{reduction} = -0.28\text{V})$$
$$\sim PO_4^{3-} + 2H_2O + 2e^- \rightarrow HPO_3^{2-} + 3OH^- \quad (E_{reduction} = -1.05\text{V})$$
$$(\text{Terpenoid} - \text{geranyl pyrophosphate Phytochemical})$$
$$\text{Overall equation: } Ag^+ + Co^{2+} + PO_4^{3-} \rightarrow AgCoPO_4$$

The appearance of surface plasmon resonance (S.P.R.) indicated the formation of nanoparticles. However, variation in the peak widths and position of the surface plasmon resonance bands (SPRB) observed could be as a result of the precursor concentrations, shape and size of nanoparticles among others [53].

From Figure 3, presence of Co in the nanohybrid caused a red shift in the absorbance edge to 427 nm and 504 nm in $AgCoPO_4$ NPs prepared from 1.0 and 2.0 mM precursor solutions respectively, compared to monometallic silver nanoparticles (400–430 nm) in our previous study [40]. Furthermore, the formation of nanoparticles with large particle sizes are expected in Figure 3a due to broad peak and longer reaction time as the growth and formation of nanoparticles is time-dependent. Also, the broad absorbance peak is a reminiscence of low aspect ratio Ag-based nanoparticles. The level of aggregation observed could be plausibly due to formation of interfacial forces in the nanocluster, as the reaction did not involve any surfactant [54]. More so, owing to the collision of small particles, and a higher concentration of the ions in the solution resulting in the increased metal ion association forming large particles.

The discrepancy in absorption spectra at different precursor mixture concentrations resulted in distinct morphological structures of the nanocluster. Slow growth rate suggests different peculiar growth mechanisms of particle formation plausibly due to strong interaction between the bioactive agents present in the biomass and the growing particles [55].

In the photoluminescence study, hybrid nanoparticles excited at 330 nm was characterised by a single emission peak in the visible region (739 nm) (Figure 4a). The vibrational relaxations of particles resulted in the emission of fluorophores observed at 739 nm. The observed emission intensity by the nanocluster was due to some allowed vertical vibrational transition in the nanohybrid [56], which is also as a result of strong local electric field intensity of the combined structure.

The optical property of the as-prepared nanoparticles was further validated using the modified mathematical expression for the optical characterisation of nanoparticles [57]:

$$I = \frac{18\pi V \varepsilon_m^{\frac{3}{2}}}{\lambda_0} \frac{\varepsilon_2}{(\varepsilon_1 + 2\varepsilon_m)^2 + \varepsilon_2^2} \tag{1}$$

Here, V is the nanoparticle volume, ε_1 is the dielectric function with its imaginary part ε_2, λ is the wavelength, ε_m the medium of permittivity and I is the intensity of absorption. This model is applied when the radii of the small spherical nanoparticles are much smaller than the wavelength of the incident light (R ~ 10 nm). The equation was simulated using the Lorentzian form of the above equation (Eq. 1). The Lorentzian fit validated the concept of particulate size distribution that was postulated by Howell et al. [58,59]. From the later results, the optimisation of the process shows that nanohybrid would increase in absorbance intensity with peak width-broadening. Based on the above, it is proposed that there may be dynamic anisotropy at the optimised state of hybrid nanoparticles (Figure 4b).

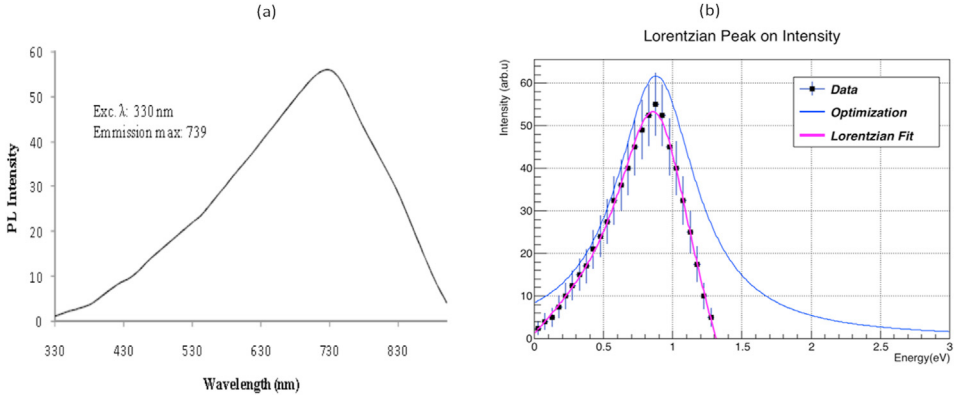

Figure 4. (a) Fluorophores emission (b) Lorentzian analysis of the hybrid N.P.s emission spectrum.

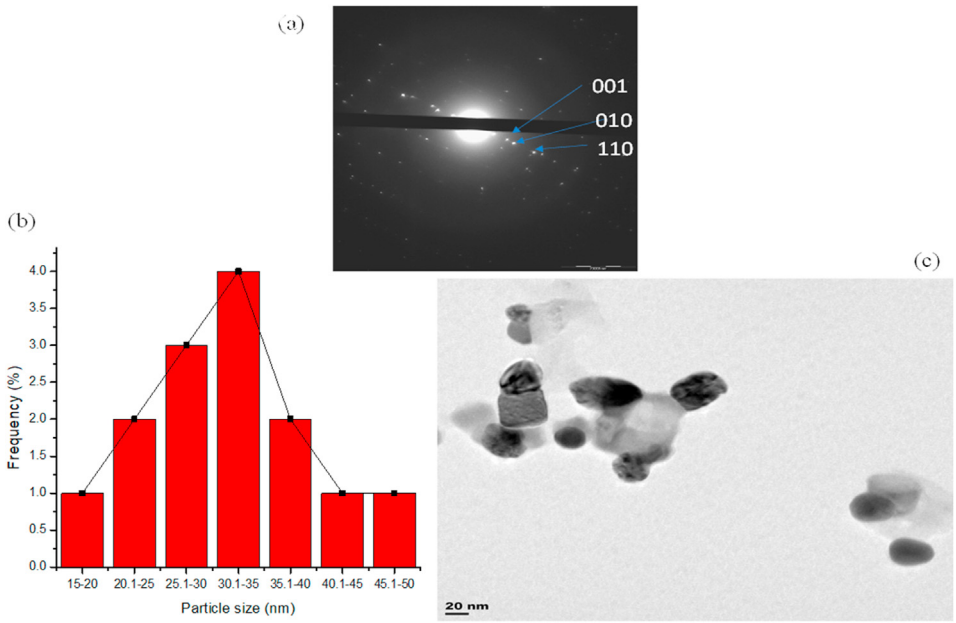

Figure 5. (a) Selected area electron diffraction (SAED) pattern of the triclinic phase $AgCoPO_4$ nanoparticles. (b) Particle size distribution histogram determined from TEM image. (c) Representative TEM images of the hybrid NPs using 1.0 mM precursor mixture.

3.4. Morphological study

Selected area electron diffraction (SAED) pattern, particle size distribution histogram and T.E.M. micrograph of the hybrid $AgCoPO_4$ nanoparticles with an average diameter of 31.94 ± 8.99 nm are shown in Figure 5. The SAED pattern conforms with XRD patterns indicating crystallinity. XRD matching indicated triclinic (anorthic) phase $AgCoPO_4$ nanoparticles (Figure 2). Further evidence of hybridisation and formation of hybrid nanoparticles with loss of crystallinity is revealed in the SAED patterns (Figure 5a), which shows that Ag and Co were fully incorporated. The T.E.M. image reveals a unique quasi-nanocubes morphology via the plant-mediated co-reduction method (Figure 5c), unlike spherical shape, which is common in plant-influenced synthesis.

Further elucidation of the $AgCoPO_4$ nanohybrid formation and composition was corroborated by E.D.X. The analysis provided localised elemental information of silver (53.99 norm. wt. %), cobalt (32.13 norm. wt.%), oxygen (6.61 norm. wt.%), phosphorus (1.68 norm. wt.%) and others accounting for surface pacifying adsorbates in the hybrid (Table 3). Carbon originated from the three metabolites present, as shown in their structures [60,61]. While the sulphur observed might be part of the impurity present. Each element in the nanoparticles released x-rays at characteristics energies by electron beam irradiation whose intensity is proportional to the concentration of each component in the nanohybrid [53,62]. However, the composition of the nanohybrid could be controlled, varying the concentration of the bio-reducing agent used.

3.5. Theory and calculation

Based on the findings above, it is important to understand the molar attenuation coefficient for the hybrid $AgCoPO_4$ nanoparticles. This process would enhance the understanding as the nanoparticles behave under corresponding wavelengths and concentration. The molar attenuation coefficient was calculated using the Beer-Lambert law, i.e.,

$$A = \varepsilon lc \tag{2}$$

Where A is the absorbance, ε is the molar attenuation coefficient of the medium, c is the molar concentration, and l is the path length (cm). The U–V absorbance presented in Figure 3 was used.

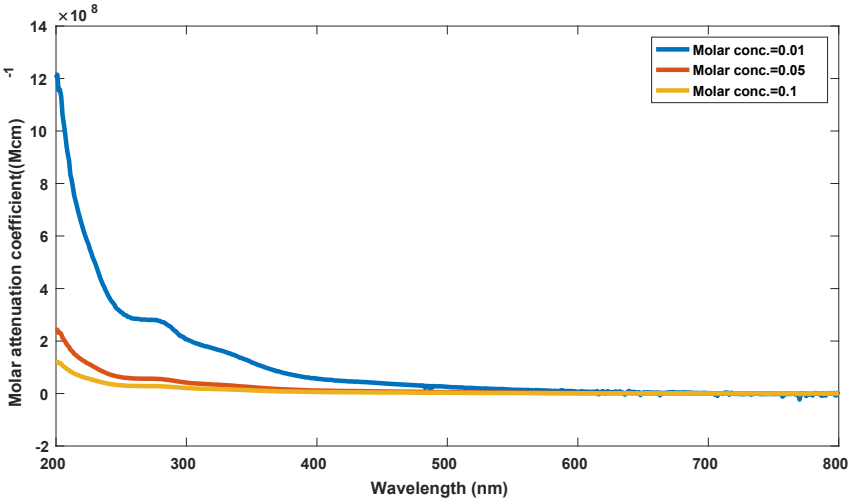

Figure 6. Molar attenuation coefficient of $AgCoPO_4$.

In this case, the path length was estimated using the mean free path λ that gives preference to the cross-section σ and the number density n of the $AgCoPO_4$ particulates. The mean free path length was estimated using:

$$\lambda \approx \frac{1}{n\sigma} \tag{3}$$

The number of density was estimated from the particle size distribution. 475 particles were calculated, as shown in Figure 6b. The number of density was estimated using:

$$n = \frac{475 \times m(kg)}{V(m^3)} \tag{4}$$

The cross-section of the particles was calculated using

$$\sigma = \pi(2R)^2 \tag{5}$$

For this calculation, the pressure was 1.01×10^{-5} pa, collision cross-section of 2.83×10^{-19} m^2, mass of the nanoparticles 0.147 kg, the height of particles in the container is 0.01 cm, where the molar concentration varied between 0.01 and 0.1M.

The estimated molar attenuation coefficient is presented in Figure 6. The molar concentrate was found to be inversely proportional to the molar attenuation coefficient (M.A.C.). In other words, the higher the molar concentration of the nanoparticles, the lower the molar attenuation coefficient expected. This information is also essential to guide the industrial-scale production of the $AgCoPO_4$. Secondly, if the molar concentration exceeds 0.1 M, the proportionality of the M.A.C. becomes very close such that the difference between succeeding M.A.C. would not be significant. Hence, the convergence of the M.A.C. will be obtained >0.1 M. The result of the M.A.C. corroborates the XRD and T.E.M. results presented above.

4. Conclusion

We have discussed the facile synthesis of triclinic (anorthic) phase $AgCoPO_4$ nanoparticles via the plant-mediated co-reduction method. Quasi-nanocube morphology was obtained via plant-mediated green synthesis method as *Canna indica* served as bio-reducing agent. Absorption studies of the $AgCoPO_4$ nanoparticles displayed distinct surface plasmon resonance band. Vibrational relaxation of the as-prepared nanoparticles also resulted in emission at 739 nm (Figure 4b). Further characterisations by T.E.M., E.D.X. and XRD strongly supported the formation of nanocube morphology via green synthesis. Phosphate originated from terpenoid, as indicated in the proposed reaction mechanism. Hence, in a quest for bioremediation, the observed enhanced S.P.R. in the absorption spectra and fluorophores emission of the nanoparticles can play an active role in optical materials as excellent absorbers of visible light. Further work on the application of this hybrid nanoparticles is ongoing.

Data availability

See supplementary tables and Mendeley data repository for the data to validate research findings.

Declarations

Author contribution statement

Anuoluwa Abimbola Akinsiku: Performed the experiments; Wrote the paper.

Olayinka Oyewale Ajani: Contributed reagents, materials, analysis tools or data.

Joseph Adeyemi Adekoya: Analyzed and interpreted the data; Wrote the paper.

Moses Eterigho Emetere: Analyzed and interpreted the data.

Enock Olugbenga Dare: Conceived and designed the experiments.

Funding statement

This research did not receive any specific grant from funding agencies in the public, commercial, or not-for-profit sectors.

Competing interest statement

The authors declare no conflict of interest.

Additional information

Supplementary content related to this article has been published online at https://doi.org/10.1016/j.heliyon.2020.e05029.

Acknowledgements

The authors recognise Mr Olusola Rotimi of the University of Western Cape, Bellville campus, Cape-Town, South Africa for the T.E.M. and E.D.X. analyses. Covenant University is highly appreciated for sponsoring this publication.

References

[1] S. Kanchi, S. Ahmed, Green Metal Nanoparticles: Synthesis, Characterisation and Their Applications, Technology & Engineering, 2018, pp. 371–373, 978-1-119-41886-3.
[2] N. Shiomi, Advances in Bioremediation of Wastewater and Polluted Soil, Science, Books on Demand, 2015, pp. 47–50. https://books.google.com.ng/books?id=pmmQDwAAQBAJ.
[3] C. Karthikeyan, K. Ramachandran, S. Sheet, D.J. Yoo, Y.S. Lee, S. kumar, A.R. Kim, Pigeon-excreta-mediated Synthesis of reduced graphene oxide (rGO)/$CuFe_2O_4$ nanocomposite and its catalytic activity toward sensitive and selective hydrogen peroxide detection, ACS Sustain. Chem. Eng. 5 (6) (2017) 4897–4905.
[4] J. Singh, T. Dutta, K. Kim, et al., 'Green' Synthesis of metals and their oxide nanoparticles: applications for environmental remediation, J. Nanobiotechnol. 16 (2018) 84.
[5] S. Rajeshkumar, L.V. Bharath, Mechanism of plant-mediated synthesis of silver nanoparticles- a review on biomolecules involved, characterisation and antibacterial Activity, Chem. Biol. Interact. 273 (2017) 219–227.
[6] D. Chunfa, C. Fei, X. Xianglin, W. Xiangjie, Y. Xiuzhi, Y. Bin, Rapid and green Synthesis of monodisperse silver nanoparticles using mulberry leaf extract, Rare Met. Mater. Eng. 47 (4) (2018) 1089–1095.
[7] N.A. Thamer, N.T. Barakat, Cytotoxic activity of green synthesis copper oxide nanoparticles using *Cordia myxa* L. aqueous extract on some breast cancer cell lines, J. Phys. Conf. 1294 (2019), 062104.
[8] J.O. Tijani, O. Ugochukwu, L.A. Fadipe, et al., One-step green synthesis of WO_3 nanoparticles using *Spondias mombin* aqueous extract: effect of solution pH and calcination temperature, Appl. Phys. A 125 (2019) 162.
[9] S. Narendhran, K.N. Reshma, Nanoparticles and their toxicology studies: a green chemistry approach, Res. Dev. Mater. Sci. 2 (3) (2017) 1–8.
[10] C. Concha, R. Cañas, J. Macuer, M.J. Torres, A.A. Herrada, F. Jamett, C. Ibáñez, Disease prevention: an opportunity to expand edible plant-based vaccines? Vaccines 5 (2) (2017) 1–23.
[11] A.N.M. Alamgir, Therapeutic use of medicinal plants and their extracts, Med. Dent. J. 2 (2018) 660.
[12] S.I. Rasmagin, V.I. Kryshtob, I.K. Novikov, Optical properties of thulium-modified silver nanoparticles, Inorg. Mater. 54 (2018) 868–872.
[13] R. Bhisey, Increased Application of Silver Nanoparticles in Healthcare Entices Demand, San Francisco, California, June 16, 2017.
[14] E. Prince, International tables for crystallography, 2016. ISBN 978-1-4020-4969-.
[15] F.T. Ling, J.E. Post, P.J. Heaney, J.D. Kubicki, C.M. Santelli, Fourier-transform infrared spectroscopy (FTIR) analysis of triclinic and hexagonal birnessites, Spectrochim. Acta 17 (2017) 32–46.
[16] M. Feng, Y. Liu, Z. Zhao, H. Huang, Z. Peng, The preparation of Fe doped triclinic-hexagonal phase heterojunction WO3 film and its enhanced photocatalytic reduction of Cr (VI) Mater, Res. Bull. 109 (2019) 168–174.
[17] R. Mandal, A. Baranwal, A. Srivastava, P. Chandra, Evolving trends in bio/chemical sensor fabrication incorporating bimetallic nanoparticles, Biosens. Bioelectron. 117 (2018) 546–561.
[18] S. Ahmed, J. Pan, M.N. Ashiq, D. Li, P. Tang, Y. Feng, Ethylene glycol-assisted fabrication and superb adsorption capacity of hierarchical porous flower-like

magnesium oxide microspheres for phosphate, Inorg. Chem. Front. 6 (2019) 1952–1961.
[19] N. Hikmah, N.F. Idrus, J. Jai, A. Hadi, Synthesis and characterisation of silver-copper core-shell nanoparticles using polyol method for antimicrobial agent, IOP Conf. Ser. Earth Environ. Sci. 36 (2016), 012050.
[20] C. Lee, N.R. Kim, J. Koo, Y.J. Lee, H.M. Lee, Cu-Ag core-shell nanoparticles with enhanced oxidation stability for printed electronics, Nanotechnology 26 (2015).
[21] N. Berahim, W.J. Basirun, B.F. Leo, M.R. Johan, Synthesis of bimetallic gold-silver (Au-Ag) nanoparticles for the catalytic reduction of 4-nitrophenol to 4-aminophenol, Catalysts 18 (2018) 412.
[22] M.K. Soni, B.K. Kukereja, K. Kohli, Combined nivolumab and ipilimumab or monotherapy in untreated melanoma, IIPP 3 (2015) 692–709.
[23] D. Castarède, E.S. Thomson, A thermodynamic description for the hygroscopic growth of atmospheric aerosol particles, Atmos. Chem. Phys. 18 (2018) 14939–14948.
[24] A. Hamdan, H. Kabbara, C. Noel, J. Ghanbaja, A. Redjaïmia, et al., Synthesis lead of two-dimensional sheets by spark discharge in liquid nitrogen, Particuology 40 (2018) 152–159. Elsevier.
[25] F.T. Rabouw, C.M. Donega, Excited-state dynamics in colloidal semiconductor nanocrystals, Top. Curr. Chem. 375 (2016) 5, 58.
[26] H. Adam, I. Juan-Carlos, L. Suljo, High-performance Ag–Co alloy catalysts for electrochemical oxygen reduction, Nat. Chem. 6 (2014) 828–834.
[27] J.A. Adekoya, S. Mlowe, E.O. Dare, M.A. Mesubi, N. Revaprasadu, Synthesis and characterisation of polyol stabilised Ag/Co allied nanocomposites, Superlattice. Microst. 78 (2015) 97–105.
[28] I. Tordjman, J.C. Guitel, M.T. Averbuch, Structure crystalline du monophosphate Ag Co $PO_4$100521-Syntheses of Hollandite type $Rb_2Cr_8O_{16}$, $K_2Cr_2V_6O_{16}$ and $K_2V_8O_{16}$, Mater. Res. Bull. 13 (1978) 983–988.
[29] J.A. Adekoya, E.O. Dare, K.O. Ogunniran, T.O. Siyanbola, O.O. Ajani, C.O. Ehi-Eromosele, R. Neerish, The effect of polyol on multiple ligand capped silver alloyed nanobimetallic particles in tri-n-octylphosphine oxide and oleic acid matrices, Adv. Nat. Sci. Nanosci. Nanotechnol. 7 (2016) 1–11.
[30] P. Liu, Y. Yao, S. Zhang, et al., Cobalt and nitrogen doped porous carbon nanofibers as an efficient electrocatalyst for high performance oxygen reduction reaction, J. Mater. Sci. Mater. Electron. 31 (2020) 7596–7605.
[31] Z. Khan, S.A. Al-Thabaiti, A.Y. Obaid, M.A. Malik, M.N. Khan, T.A. Khan, Cobalt@silver bimetallic nanoparticles: solution based seedless surfactant assisted synthesis, optical properties, and morphology, J. Mol. Liq. 222 (2016) 272–278.
[32] L. Ai, X. Liu, J. Jiang, Synthesis of loofah sponge carbon supported bimetallic silver–cobalt nanoparticles with enhanced catalytic activity towards hydrogen generation from sodium borohydride hydrolysis, J. Alloys Compd. 625 (2015) 164–170.
[33] M.N.I. Anuar, J. Andas, Synthesis and characterisation of biomass supported Ag, Co and Ag-Co nanoparticles, Mater. Sci. Forum 857 (2016) 480–484.
[34] A. El-Hela, N.M. Abdelhady, M.H. Gonaid, K.A. Badr, antioxidant, cytotoxic and antimicrobial activities of crude and green synthesised silver nanoparticles' extracts of *Crataegus sinaica Boiss*. Leaves, Int. J. Pharmaceut. Sci. Rev. Res. 45 (1) (2017) 223–232. Available online at, www.globalresearchonline.net.
[35] G. Bagherzade, M.T. Mohmmad, H. Namaei, Green synthesis of silver nanoparticles using aqueous extract of saffron (*Crocus sativus* L.) wastages and its antibacterial activity against six bacteria, APJTB 7 (3) (2017) 227–233.
[36] M. Sakira, M.S. Onses, Solid substrates decorated with Ag nanostructures for the catalytic degradation of methyl orange, Results Phys. 12 (2019) 1133–1141.
[37] M.K. Singh, M. Kuncha, V.L. Nayak, A.V.S. Sarma, M.J.M. Kumar, R. Sistla, An innovative in situ method of creating hybrid dendrimer nano-assembly: an efficient next-generation dendritic platform for drug delivery, Nanomedicine: N.B.M. 2019 21 (2019) 102043.
[38] O. Ivashchenko, T. Tomila, N. Ulyanchich, T. Yarmola, I.U. Varova, Fourier-Transform Infrared Spectroscopy of antibiotic loaded Ag-free and Ag-doped hydroxyapatites, Adv. Sci. Eng. Med. 6 (2014) 193–202.
[39] Q. Wang, C. Xu, M. Ming, Y. Yang, B. Xu, Y. Wang, Y. Zhang, J. Wu, G. Fan, In situ formation of AgCo stabilised on graphitic carbon nitride and concomitant hydrolysis of ammonia borane to hydrogen, Nanomaterials (Basel) 8 (5) (2018) 280.
[40] A.A. Akinsiku, E.O. Dare, K.O. Ajanaku, J.A. Adekoya, S.O. Alayande, A.O. Adeyemi, Synthesis of silver nanoparticles by plant-mediated green method: optical and biological properties, J. Bionanoscience 10 (3) (2016) 171–180.
[41] A.A. Akinsiku, E.O. Dare, K.O. Ajanaku, O.O. Ajani, J.A.O. Olugbuyiro, T.O. Siyanbola, O. Ejilude, M.E. Emetere, Modeling and Synthesis of Ag and Ag/Ni allied bimetallic nanoparticles by green method: optical and biological Properties, Int. J. Biomater. (2018) 9658080.
[42] T.V. Surendra, S.M. Roopan, N.A. Al-Dhabi, M.V. Arasu, G. Sarkar, K. Suthindhiran, Vegetable peel waste for the production of ZnO nanoparticles and its toxicological efficiency, antifungal, hemolytic, and antibacterial activities, Nanoscale Res. Lett. 11 (2016) 546.
[43] P. Tu, J. Jiang, H. Xiao, Green Synthesis of aryl thioethers through Cu-catalysed C-S coupling of thiols and aryl boronic acids in water, Wuhan Univ. Technol.-Mat. Sci. Edit. 34 (2019) 987.
[44] M.N. Abdullahi, S. Ilyas, H. Ibrahim, Evaluation of phytochemical screening and analgesic activity of aqueous extract of the leaves of *Microtrichia perotitii* dc (Asteraceae) in mice using hotplate method, Med. Plant Res. 3 (2013) 37–43.
[45] T.T. Alawode, L. Lajide, B.J. Owolabi, M.T. Olaleye, Studies on in vitro antioxidant and anti-inflammatory activities *of Crinum jagus* Leaves and bulb extracts, IJBcRR 28 (1) (2019) 1–9.
[46] A. Al-AsfarZoyaZaheer, E.S. Aazam, Eco-friendly green Synthesis of Ag@Fe bimetallic nanoparticles: antioxidant, antimicrobial and photocatalytic degradation of bromothymol blue, J. Photochem. Photobiol., B: Biol. Photochem. Photobiol. B, Biol. 185 (2018) 143–152.
[47] A.A. Akinsiku, K.O. Ajanaku, J.A. Adekoya, E.O. Dare, Green synthesis, characterisation of silver nanoparticles using *Canna indica* and *Senna occidentalis* leaf extracts, Int. Conf. Afri. Dev. Issues (2015).
[48] H. Xiao, 1Y. Zhang, M. Wang, Discovery and engineering of cytochrome P450s for terpenoid biosynthesis-a review, Trends Biotechnol. 37 (6) (2019) 618–631.
[49] A. Krasnok, M. Tymchenko, A. Alù, Non-linear metasurfaces: a paradigm shift in non-linear optics, Res. Rev. 21 (2018) 8–21.
[50] A. Akinsiku, Green Synthesis of AgCoPO4 Nanoparticles: Optical Studies and Theoretical Modelling, Mendeley Data, 2020, p. V1.
[51] S. Rajeshkumar, Synthesis of silver nanoparticles using fresh bark of *Pongamia pinnata* and characterisation of its antibacterial activity against gram-positive and gram-negative pathogens, Resour. Technol. 2 (1) (2016) 30–35.
[52] H. Duan, D. Wang, Y. Li, Green chemistry for nanoparticle synthesis- a review, Chem. Soc. Rev. 44 (2015) 5778–5792.
[53] P. Rameshthangam, J.P. Chitra, Synergistic anticancer effect of green synthesised nickel nanoparticles and quercetin extracted from *Ocimum sanctum* leaf extract, J. Mater. Sci. Technol. 34 (3) (2018) 508–522.
[54] R. Wu, L. Hao, X. Yu, et al., Core-shell structure of $NaYF_4$@SiO_2@Au nanocomposite of synthesis and characterisation with mechanisms research, J. Wuhan Univ. Technol.-Materials Sci. Ed. 34 (2019) 900–905.
[55] Z. Weia, D. Thusharaa, Z. Li, Z. hang, Y. Liu, X. Lu, Ligand-controlled fabrication of core-shell PdNi bimetallic nanoparticles as a highly efficient hydrogenation catalyst, Catal. Commun. 98 (2017) 61–65.
[56] M. Irfan, T. Ahmad, M. Moniruzzaman, S. Bhattacharjee, B. Abdulla, Size and stability modulation of ionic liquid functionalised gold nanoparticles synthesised using *Elaeis guineensis* (oil palm) kernel extract, Arab J. Chem. 13 (1) (2020) 75–85.
[57] A.F. Rahim, M.R. Hashim, N.K. Ali, High sensitivity of palladium on porous silicon M.S.M. photodetector, Phys. B Condens. Matter 406 (4) (2011) 1034–1037.
[58] R.C. Howell, T. Proffen, Steven D. Conradson, Pair distribution function and structure factor of spherical particles, Phys. Rev. B 73 (2006) 94–107.
[59] K.T. Lin, J.W. Silze, Relation of molecular structure to Franck–Condon bands in the visible-light absorption spectra of symmetric cationic cyanine dyes, Spectrochim. Acta Mol. Biomol. Spectrosc. 142 (2015) 210–219.
[60] T. Aniszewski, Alkaloids, second ed., Elsevier, 2015, pp. 99–193.
[61] N.V. Bhagavan, Simple Carbohydrates, Elsevier, 2002, pp. 133–151.
[62] D. Latha, S. Sampurnam, C. Arulvasu, P. Prabu, K. Govindaraju, Biosynthesis and characterisation of gold nanoparticle from Justicia adhatoda and its catalytic activity, Mater. Today: Proceedings 5 (2) (2018) 8968–8972.